Arabian Journal for Science and Engineering (2020) 45:3015–3024
https://doi.org/10.1007/s13369-019-04249-z

RESEARCH ARTICLE - COMPUTER ENGINEERING AND COMPUTER SCIENCE

Integrated WiFi/MEMS Indoor Navigation Based on Searching Space Limiting and Self-calibration

Yi Cui[1] · Yongbo Zhang[1,2] · Zhihua Wang[1] · Huimin Fu[1]

Received: 1 March 2019 / Accepted: 11 November 2019 / Published online: 18 November 2019

Abstract
Indoor navigation has been increasingly popular over the last few years. However, it still faces plenty of challenges and remains a conundrum. This paper proposes a novel improved WiFi/MEMS integration solution for indoor navigation. In WiFi fingerprinting scheme, a novel searching space limiting method is originally presented and associated with a mean filter to improve computation efficiency and positioning accuracy, compared with the traditional weighted K-nearest neighbors method. In pedestrian dead-reckoning part, an attitude determination extended Kalman filter with correlated process and measurement noise is presented to obtain an accurate long-term heading and the average positioning error decreases significantly as a result. Furthermore, the self-calibration Kalman filter approach is introduced into indoor navigation field in WiFi/MEMS integration stage and a novel Kalman filter system is originally designed to fuse the information effectively. The navigation performance of the proposed WiFi/MEMS algorithm has been validated by indoor experiments, and the average positioning error is less than 0.6 m when the number of selected APs is optimal.

Keywords Indoor navigation · WiFi · MEMS · Self-calibration Kalman filter · Weighted K-nearest neighbors

1 Introduction

In recent years, indoor navigation has gained a significant attention from researchers. Indoor navigation can be traced back before smartphones came into existence [1]. RADAR [2] and Horus [3] were examples. Since people spend about 70% of their time indoors [4], the demand of indoor navigation is increasing rapidly. However, signals from the widely used Global Navigation Satellite Systems (GNSS) are often not hearable in indoor environments [5]. As a result, indoor navigation remains a difficult problem. To overcome this conundrum, researchers have developed various approaches using inertial measurement unit (IMU) [6], magnetic field [7], ultrasonic [8], radio-frequency (RF) ID tags [9], FM [10], WiFi [11], etc.

Among the above methods, WiFi-based positioning technique has been much favored in indoor environments. The advantages of WiFi are low device cost, wide infrastructure deployment and high positioning accuracy [5]. WiFi indoor navigation approaches are essentially divided into two categories: trilateration and fingerprinting [12]. In the former, a radio propagation model (RPM) is established and the distance between WiFi access points (AP) and the mobile user (MU) is estimated through RPM and the received signal strength (RSS) [13]. Due to the complexity of indoor environments, an accurate RPM cannot be found to describe propagation characteristics of WiFi signals inside buildings [14]. In the fingerprinting method, there are usually two phases: offline and online phases. In the offline stage, the main work is setting the locations of many reference points (RPs) as the shape of the square grid (each RP receives signal strength data from multiple APs) and storing the signal strength data with position coordinates of RPs in the database. In the online stage, the MU detects RSSs at positioning points and uses various matching algorithms to identify his locations by comparing RSS measurements with the reference data [12, 14]. Although fingerprinting approach needs to establish fingerprint database at the early stage, it can effectively avoid the influence of building structure. Besides, it does not require WiFi APs to be known in advance [15]. Therefore, it has gained much attention [16]. In this paper,

✉ Yongbo Zhang
zhangyongbo@buaa.edu.cn

[1] Research Center of Small Sample Technology, Beihang University, Beijing 100191, China

[2] Aircraft and Propulsion Laboratory, Ningbo Institute of Technology, Beihang University, Ningbo 315100, China

a novel WiFi fingerprinting method with searching space limiting and mean filtering is proposed to achieve better performance (including higher computation efficiency and higher positioning accuracy) than traditional ones.

Since most of the current smartphones are equipped with inertial sensors (including accelerometers and gyroscopes), microelectromechanical system (MEMS) sensor-based navigation is becoming a popular relative and self-contained positioning technique [5]. MEMS sensors have the virtue of lower cost and small form factor [17]. For consumer portable devices, dead reckoning (DR) is commonly the algorithm applied to position with inertial sensors [16]. There are two categories of DR algorithms: inertial navigation system (INS) mechanism and pedestrian dead reckoning (PDR). INS is a system of calculating velocity by integration of the total acceleration and computing position by integration of the resultant velocity [18]. It has a simple structure and strong autonomy and is commonly used in vehicle navigation [19]. However, the navigation error of INS will appear unconstrained divergence over time [20]. In order to improve the navigation performance for pedestrians, PDR is developed to reduce the accumulated errors [21]. The basic principle of PDR is that the current location can be found out by calculating moved distance with heading angle from initial location [22]. PDR uses IMU to detect when the MU takes footsteps and how the direction changes between footsteps [23]. So far, calculating an accurate long-term heading remains the most challenging problem in PDR [24]. In this paper, a novel integrated MEMS solution applying Kalman filtering with correlated process and measurement noise is proposed to achieve better performance (much higher positioning accuracy) than traditional ones.

For the integration of WiFi and MEMS, there are a number of existed researches. Tian et al. [5] proposed a novel smartphone-based integrated WiFi/MEMS positioning algorithm based on the robust extended Kalman filter (EKF) in a multi-floor environment. Zhuang and El-Sheimy [25] originally proposed a pedestrian navigator based on tightly coupled integration of low-cost MEMS sensors and WiFi for handheld devices. Zhuang et al. [26] presented a two-filter integration for MEMS sensors and WiFi fingerprinting where a smoothed constrained fingerprinting was obtained. In our previous research [27], we proposed a novel WiFi/MEMS integration structure for indoor navigation using two-stage EKF. Using the same data from WiFi/MEMS sensors, different information fusion structures may lead to various results [16]. In the current study, the self-calibration Kalman filter (SKF) approach is introduced into indoor navigation field for WiFi/MEMS integration and a novel Kalman filter system is designed to fuse the information effectively. As a result, satisfactory navigation performance is achieved.

The rest of this paper is organized as follows. Section 2 presents the system overview. The WiFi solution and PDR solution are illustrated in Sects. 3 and 4, respectively. In Sect. 5, the SKF-based integration of WiFi and MEMS is analyzed. Section 6 provides details of experiments and results. Section 7 makes the conclusion.

2 System Overview

The block diagram of the proposed WiFi/MEMS structure for indoor navigation is shown in Fig. 1.

The proposed system mainly includes three modules: WiFi-based navigation, PDR-based navigation, and WiFi/MEMS integration. In WiFi solution, RSS values pass to the fingerprinting scheme to generate the MU position and a novel searching space limiting method is originally presented. In PDR solution, an attitude determination EKF with correlated process and measurement noise is presented using the gyroscope and accelerometer data, and then PDR algorithm is applied to calculate the position of the MU. In WiFi/MEMS integration, the SKF approach is applied to fuse the above information and finally achieve high-accuracy indoor navigation.

3 WiFi-Based Navigation

In WiFi fingerprinting scheme, to estimate the position of the MU, different matching algorithms have been presented [28]. There are probabilistic approaches [29, 30], deterministic approaches [31, 32], and neural networks [33, 34]. Among them, K-nearest neighbor (KNN) is one of the top algorithms in data mining [35]. As an effective method to determine the most important objects of interests, the KNN query is designed to find the top k closest objects to a specified query point,

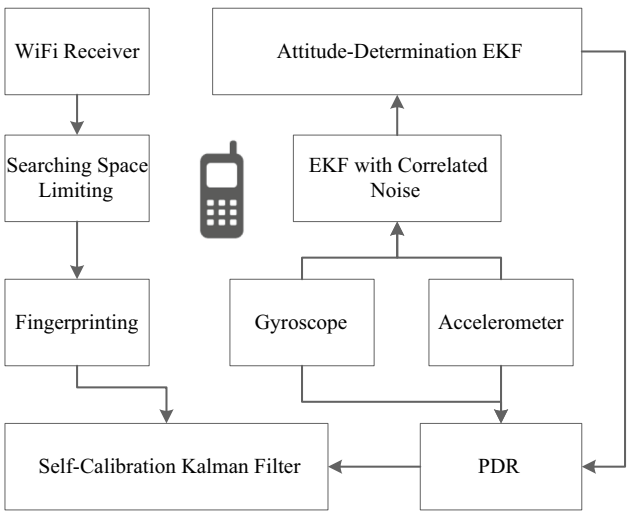

Fig. 1 Block diagram

given a set of objects and a distance metric [36]. There are different types of distance metrics [12, 32, 37, 38]. Furthermore, weighted K-nearest neighbor (WKNN) method [39] has been developed. According to WKNN, the MU position is calculated utilizing the weighted mean of position coordinates of the k RPs. There are various methods to determine weights [14].

In KNN and WKNN algorithms, it is necessary to search the overall space and go through the whole database fingerprints, which usually means low efficiency and unacceptable computation time. In addition, this increases the probability of mismatching and thereby reduces the navigation accuracy. In the current study, the searching space is limited into a circle determined with the information of the latest positioning point. Firstly, as a single position may correspond to several RSS measurements, the method of inverse regression analysis and data fusion proposed in the literature [40] is introduced into WiFi fingerprinting navigation for a more accurate estimation as follows.

Let x be the argument and y be the random variable. There is a relationship between x and y as follows:

$$y = a + bx + \varepsilon \tag{1}$$

$$\varepsilon \sim N(0, \sigma^2), \tag{2}$$

where a, b, and σ^2 are undetermined parameters independent of x.

Suppose $(x'_1, y'_1), (x'_2, y'_2), \cdots, (x'_{n'}, y'_{n'})$ are a sample obtained through n' independent trials. Then, the estimates of a, b, and σ can be obtained as follows:

$$\hat{a} = \bar{y}' - \hat{b}\bar{x}' \tag{3}$$

$$\hat{b} = L_{xx}^{-1} L_{xy} \tag{4}$$

$$\hat{\sigma} = \sqrt{\sum_{i=1}^{n'} \frac{\left(y'_i - \hat{a} - \hat{b}x'_i\right)^2}{n' - 2}}, \tag{5}$$

where

$$\bar{x}' = \frac{1}{n'} \sum_{i=1}^{n'} x'_i \tag{6}$$

$$\bar{y}' = \frac{1}{n'} \sum_{i=1}^{n'} y'_i \tag{7}$$

$$L_{xx} = \sum_{i=1}^{n'} \left(x'_i - \bar{x}'\right)^2 \tag{8}$$

$$L_{xy} = \sum_{i=1}^{n'} \left(x'_i - \bar{x}'\right)\left(y'_i - \bar{y}'\right). \tag{9}$$

Assume n independent measurements are conducted under the same condition, and n values of variable y $(y_1, y_2, \ldots, y_n)$ are gained. Then, the estimate of x can be obtained as follows:

$$\hat{x} = (\bar{y} - \hat{a}) \Big/ \hat{b}, \tag{10}$$

where

$$\bar{y} = \frac{1}{n} \sum_{i=1}^{n} y_i. \tag{11}$$

When $b > 0$, the one-side lower and upper confidence limits of x at the confidence level of P can be calculated by

$$\hat{a} + \hat{b}x_{\mathrm{L}} + u_{\mathrm{P}} S \Big/ \sqrt{n} = \bar{y} \tag{12}$$

$$\hat{a} + \hat{b}x_{\mathrm{U}} - u_{\mathrm{P}} S \Big/ \sqrt{n} = \bar{y}, \tag{13}$$

where x_{L} and x_{U} are the one-side lower and upper confidence limits of x, respectively; u_{P} is the P percentage point of the standard normal distribution; S is given by

$$S^2 = \frac{1}{n' + n - 3} \left[\left(n' - 2\right)\hat{\sigma}^2 + \sum_{i=1}^{n} \left(y_i - \bar{y}\right)^2 \right]. \tag{14}$$

When $b < 0$, the one-side lower and upper confidence limits of x at the confidence level of P can be calculated by

$$\hat{a} + \hat{b}x_{\mathrm{L}} - u_{\mathrm{P}} S \Big/ \sqrt{n} = \bar{y} \tag{15}$$

$$\hat{a} + \hat{b}x_{\mathrm{U}} + u_{\mathrm{P}} S \Big/ \sqrt{n} = \bar{y}. \tag{16}$$

In this paper, a novel searching space limiting method is proposed based on the above approach. In the proposed method, a probability circle of the MU's position is determined with the information of the latest positioning point and the searching space is limited into the circle. The center of the circle is located at the latest positioning point, and its radius is determined through the following analysis.

When a test point is located, its position coordinates can be regarded as known values. Selecting n' reference points which have the shortest RSS distances (D_i) to the test point, their spatial distances to the test point (L_i) can be calculated. It is found that $\ln D_i$ varies in good linearity with $\ln L_i$. Therefore, a line mode is established as shown in Eqs. (17) and (18):

$$\ln D = a + b \ln L + \varepsilon \tag{17}$$

$$\varepsilon \sim N(0, \sigma^2), \tag{18}$$

where the parameters a, b, and σ can be estimated according to Eqs. (3)–(5).

When locating the next test point, the RSS distance between next point and this point (D^*) can be calculated easily. According to Eqs. (13) and (14), the one-side upper limit of $\ln L^*$ is obtained as follows:

$$(\ln L^*)_{\mathrm{U}} = \frac{1}{\hat{b}}\left(\ln D^* + u_{\mathrm{P}} S - \hat{a}\right), \tag{19}$$

where

$$S^2 = \hat{\sigma}^2 = \sum_{i=1}^{n'} \frac{\left(\ln D_i - \hat{a} - \hat{b} \ln L_i\right)^2}{n' - 2}. \tag{20}$$

Therefore, we have the one-side upper limit of the spatial distance between these two points (L_U^*) as follows:

$$L_{\mathrm{U}}^* = \exp\left[\frac{1}{\hat{b}}\left(\ln D^* + u_{\mathrm{P}} S - \hat{a}\right)\right]. \tag{21}$$

A circle with the radius of L_{U}^* at this point is a probability circle of the MU's position at the next point. Then, the position of the next point can be calculated within the scope of RPs in the circle plus this point. Thus, the position of this point is taken into account. Therefore, the area of searching space is significantly reduced and the navigation accuracy is increased.

In WiFi fingerprinting positioning, there is a common phenomenon named reciprocating motion, as shown in Fig. 2a. The positioning points often flock together and bounce around, resulting in poor positioning accuracy. In this paper, a seven-order mean filter is applied to the original positioning results for smoothing. After filtered, the phenomenon of reciprocating motion has been eliminated greatly, as shown in Fig. 2b. The positioning points become consistent, and the positioning accuracy is increased.

4 PDR-Based Navigation

Generally, a PDR system consists of three parts: step detection, step length estimation, and heading calculation. PDR algorithm is illustrated as follows [21]:

$$\begin{cases} x_i = x_{i-1} + s_i \cos \psi_i \\ y_i = y_{i-1} + s_i \sin \psi_i \end{cases}, \tag{22}$$

where x_i, y_i are position coordinates of the MU at the ith step, s_i is the estimated step length of the ith step, and ψ_i is the heading angle of the ith step.

As described above, calculating an accurate long-term heading is the most challenging issue in PDR. In this paper, the attitude determination EKF in [27] is applied to estimate the heading of the pedestrian using the data obtained from triaxial gyroscopes and accelerometers as follows.

The state vector is written as

$$\mathbf{D}_k = \left[\psi_k \, \theta_k \, \gamma_k\right]^T, \tag{23}$$

where ψ is the heading angle, θ is the pitching angle, and γ is the roll angle.

The system model is as follows:

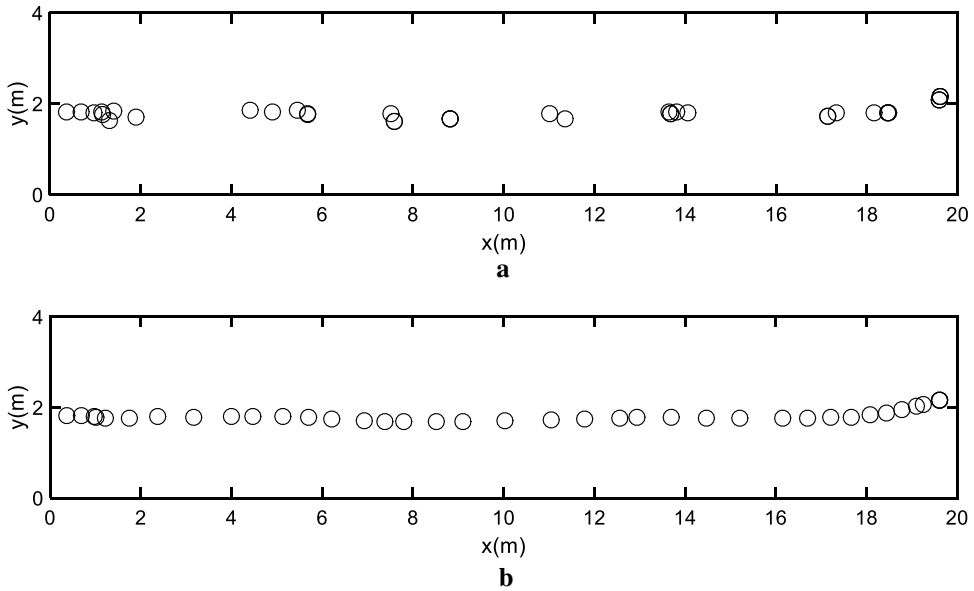

Fig. 2 WiFi positioning results **a** before filtered, **b** after filtered

$$\begin{cases} \psi_k = \psi_{k-1} + \left(\frac{\sin\gamma_{k-1}}{\cos\theta_{k-1}}\omega_{x,k-1} - \frac{\cos\gamma_{k-1}}{\cos\theta_{k-1}}\omega_{z,k-1}\right)\Delta t + w_{\psi,k-1} \\ \theta_k = \theta_{k-1} + \left(\cos\gamma_{k-1}\omega_{x,k-1} + \sin\gamma_{k-1}\omega_{z,k-1}\right)\Delta t + w_{\theta,k-1} \\ \gamma_k = \gamma_{k-1} + \left(\sin\gamma_{k-1}\tan\theta_{k-1}\omega_{x,k-1} + \omega_{y,k-1} - \cos\gamma_{k-1}\tan\theta_{k-1}\omega_{z,k-1}\right)\Delta t + w_{\gamma,k-1} \end{cases}, \tag{24}$$

where $\omega_x, \omega_y, \omega_z$ are angular velocities observed in the carrier coordinate system, $w_\psi, w_\theta, w_\gamma$ are noise, and Δt is the sampling interval.

The measurement vector is written as

$$\mathbf{A}_k = \left[a_{x,k}\, a_{y,k}\, a_{z,k}\right]^T, \tag{25}$$

where a_x, a_y, a_z are accelerations observed in the carrier coordinate system.

The measurement model is as follows:

$$\mathbf{A}_k = \mathbf{T}_k^{-1}[0\,0\,1]^T + \mathbf{v}_k, \tag{26}$$

where $\mathbf{T}_k$ is the direction cosine matrix calculated by Eq. (27) and $\mathbf{v}_k$ is the noise.

$$\mathbf{T}_k = \begin{bmatrix} \cos\psi_k & -\sin\psi_k & 0 \\ \sin\psi_k & \cos\psi_k & 0 \\ 0 & 0 & 1 \end{bmatrix}\begin{bmatrix} \cos\theta_k & 0 & \sin\theta_k \\ 0 & 1 & 0 \\ -\sin\theta_k & 0 & \cos\theta_k \end{bmatrix}\begin{bmatrix} 1 & 0 & 0 \\ 0 & \cos\gamma_k & -\sin\gamma_k \\ 0 & \sin\gamma_k & \cos\gamma_k \end{bmatrix}. \tag{27}$$

Since perturbations while walking affect both gyroscopes and accelerometers, the process noise and measurement noise are correlated, which has been ignored by most previous studies. Therefore, in the current study, a novel navigation algorithm is proposed as follows based on the EKF with correlated process and measurement noise [41].

The navigation system is given by

$$\begin{aligned} \mathbf{D}_k &= f_{k-1}\left(\mathbf{D}_{k-1}, \mathbf{u}_{k-1}, \mathbf{w}_{k-1}\right) \\ \mathbf{A}_k &= h_k\left(\mathbf{D}_k, \mathbf{v}_k\right) \\ \mathbf{w}_k &\sim \left(0, \mathbf{Q}_k\right) \\ \mathbf{v}_k &\sim \left(0, \mathbf{R}_k\right) \\ E\left[\mathbf{w}_k\mathbf{w}_j^T\right] &= \mathbf{Q}_k\delta_{k-j} \\ E\left[\mathbf{v}_k\mathbf{v}_j^T\right] &= \mathbf{R}_k\delta_{k-j} \\ E\left[\mathbf{w}_k\mathbf{v}_j^T\right] &= \mathbf{M}_k\delta_{k-j+1}, \end{aligned} \tag{28}$$

where $f_{k-1}(\cdot)$ is the system model defined in Eq. (24), $h_k(\cdot)$ is the measurement model defined in Eq. (26), $\mathbf{D}_k$ is the state vector, $\mathbf{A}_k$ is the measurement vector, $\mathbf{u}_{k-1} = \left[\omega_{x,k-1}\, \omega_{y,k-1}\, \omega_{z,k-1}\right]^T$, $\mathbf{w}_{k-1}$, and $\mathbf{v}_k$ are noise. δ_{k-j} is the Kronecker delta function, $\delta_{k-j} = 1$ if $k = j$, and $\delta_{k-j} = 0$ if $k \neq j$.

The EKF is initialized as

$$\begin{aligned} \hat{\mathbf{D}}_0^+ &= E\left(\mathbf{D}_0\right) \\ \mathbf{P}_0^+ &= E\left[\left(\mathbf{D}_0 - \hat{\mathbf{D}}_0^+\right)\left(\mathbf{D}_0 - \hat{\mathbf{D}}_0^+\right)^T\right]. \end{aligned} \tag{29}$$

For $k = 1, 2, \cdots$, perform the following steps:

(a) Compute the following partial derivative matrices:

$$\begin{aligned} \mathbf{F}_{k-1} &= \left.\frac{\partial f_{k-1}}{\partial \mathbf{D}}\right|_{\hat{\mathbf{D}}_{k-1}^+} \\ \mathbf{L}_{k-1} &= \left.\frac{\partial f_{k-1}}{\partial \mathbf{w}}\right|_{\hat{\mathbf{D}}_{k-1}^+}. \end{aligned} \tag{30}$$

(b) Perform the time update of the state estimate and estimation error covariance as follows:

$$\begin{aligned} \mathbf{P}_k^- &= \mathbf{F}_{k-1}\mathbf{P}_{k-1}^+\mathbf{F}_{k-1}^T + \mathbf{L}_{k-1}\mathbf{Q}_{k-1}\mathbf{L}_{k-1}^T \\ \hat{\mathbf{D}}_k^- &= f_{k-1}\left(\hat{\mathbf{D}}_{k-1}^+, \mathbf{u}_{k-1}, 0\right). \end{aligned} \tag{31}$$

(c) Compute the following partial derivative matrices:

$$\begin{aligned} \mathbf{H}_k &= \left.\frac{\partial h_k}{\partial \mathbf{D}}\right|_{\hat{\mathbf{D}}_k^-} \\ \mathbf{N}_k &= \left.\frac{\partial h_k}{\partial \mathbf{v}}\right|_{\hat{\mathbf{D}}_k^-}. \end{aligned} \tag{32}$$

(d) Perform the measurement update of the state estimate and estimation error covariance as follows:

$$\begin{aligned} \mathbf{K}_k &= \left(\mathbf{P}_k^-\mathbf{H}_k^T + \mathbf{M}_k\right)\left(\mathbf{H}_k\mathbf{P}_k^-\mathbf{H}_k^T + \mathbf{H}_k\mathbf{M}_k + \mathbf{M}_k^T\mathbf{H}_k^T + \mathbf{N}_k\mathbf{R}_k\mathbf{N}_k^T\right)^{-1} \\ \hat{\mathbf{D}}_k^+ &= \hat{\mathbf{D}}_k^- + \mathbf{K}_k\left[\mathbf{A}_k - h_k\left(\hat{\mathbf{D}}_k^-, 0\right)\right] \\ \mathbf{P}_k^+ &= \mathbf{P}_k^- - \mathbf{K}_k\left(\mathbf{H}_k\mathbf{P}_k^- + \mathbf{M}_k^T\right). \end{aligned} \tag{33}$$

Figure 3 depicts the comparison of heading calculation utilizing filters with correlated noise and uncorrelated noise. As shown, the heading estimation using traditional attitude determination EKF (with uncorrelated noise) deviates from the actual value obviously. When applying the proposed PDR-based navigation algorithm (with correlated noise), the heading estimation fits the actual value well. Therefore, more accurate long-term heading calculation is obtained and positioning accuracy is improved.

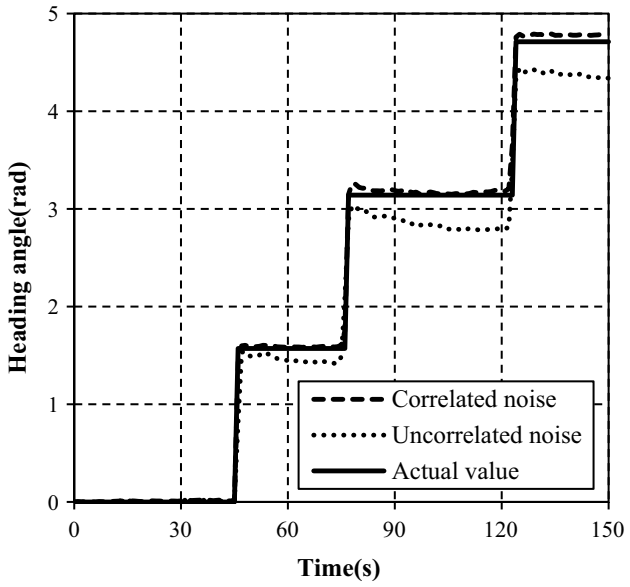

Fig. 3 Heading calculation in PDR

5 SKF-Based Integration

The integration stage of the navigation algorithm is proposed in this section utilizing the information from WiFi and MEMS positioning results. To obtain an accurate and stable estimation, the SKF method proposed in [42] is introduced into indoor navigation field as follows:

Suppose we have a system given by

$$\begin{aligned}
\mathbf{X}_k &= \mathbf{F}_{k-1}\mathbf{X}_{k-1} + \mathbf{G}_{k-1}\mathbf{u}_{k-1} + \mathbf{b}_{k-1} + \mathbf{w}_{k-1} \\
\mathbf{Y}_k &= \mathbf{H}_k\mathbf{X}_k + \mathbf{v}_k \\
\mathbf{w}_k &\sim \left(0, \mathbf{Q}_k\right) \\
\mathbf{v}_k &\sim \left(0, \mathbf{R}_k\right) \\
E\left[\mathbf{w}_k\mathbf{w}_j^T\right] &= \mathbf{Q}_k\delta_{k-j} \\
E\left[\mathbf{v}_k\mathbf{v}_j^T\right] &= \mathbf{R}_k\delta_{k-j} \\
E\left[\mathbf{w}_k\mathbf{v}_j^T\right] &= 0,
\end{aligned} \tag{34}$$

where $\mathbf{X}_k$ is the state vector, $\mathbf{Y}_k$ is the measurement vector, $\mathbf{u}_{k-1}$ is a known input, $\mathbf{b}_{k-1}$ is an unknown input, $\mathbf{w}_{k-1}$ and $\mathbf{v}_k$ are noise. δ_{k-j} is the Kronecker delta function.

The SKF is initialized as

$$\begin{aligned}
\hat{\mathbf{X}}_0^+ &= E\left(\mathbf{X}_0\right) \\
\mathbf{P}_0^+ &= E\left[\left(\mathbf{X}_0 - \hat{\mathbf{X}}_0^+\right)\left(\mathbf{X}_0 - \hat{\mathbf{X}}_0^+\right)^T\right].
\end{aligned} \tag{35}$$

For $k = 1, 2$, the Kalman filter equations are given as

$$\begin{aligned}
\mathbf{P}_k^- &= \mathbf{F}_{k-1}\mathbf{P}_{k-1}^+\mathbf{F}_{k-1}^T + \mathbf{Q}_{k-1} \\
\mathbf{K}_k &= \mathbf{P}_k^-\mathbf{H}_k^T\left(\mathbf{H}_k\mathbf{P}_k^-\mathbf{H}_k^T + \mathbf{R}_k\right)^{-1} \\
\hat{\mathbf{X}}_k^- &= \mathbf{F}_{k-1}\hat{\mathbf{X}}_{k-1}^+ + \mathbf{G}_{k-1}\mathbf{u}_{k-1} \\
\hat{\mathbf{X}}_k^+ &= \hat{\mathbf{X}}_k^- + \mathbf{K}_k\left(\mathbf{Y}_k - \mathbf{H}_k\hat{\mathbf{X}}_k^-\right) \\
\mathbf{P}_k^+ &= \left(\mathbf{I} - \mathbf{K}_k\mathbf{H}_k\right)\mathbf{P}_k^-,
\end{aligned} \tag{36}$$

where $\mathbf{I}$ is an identity matrix.

For $k = 3, 4, \ldots$, the SKF equations are given as

$$\begin{aligned}
\mathbf{P}_k^- &= \left(\mathbf{I} + \mathbf{F}_{k-1}\right)\mathbf{P}_{k-1}^+\left(\mathbf{I} + \mathbf{F}_{k-1}\right)^T + \mathbf{F}_{k-2}\mathbf{P}_{k-2}^+\mathbf{F}_{k-2}^T - \left(\mathbf{I} + \mathbf{F}_{k-1}\right)\mathbf{S}_{k-1}\mathbf{F}_{k-2}^T \\
&\quad - \mathbf{F}_{k-2}\mathbf{S}_{k-1}^T\left(\mathbf{I} + \mathbf{F}_{k-1}\right)^T - \left(\mathbf{I} + \mathbf{F}_{k-1}\right)\left(\mathbf{I} - \mathbf{K}_{k-1}\mathbf{H}_{k-1}\right)\mathbf{Q}_{k-2} - \\
&\quad \mathbf{Q}_{k-2}\left(\mathbf{I} - \mathbf{K}_{k-1}\mathbf{H}_{k-1}\right)^T\left(\mathbf{I} + \mathbf{F}_{k-1}\right)^T + \mathbf{Q}_{k-1} + \mathbf{Q}_{k-2} \\
\mathbf{K}_k &= \mathbf{P}_k^-\mathbf{H}_k^T\left(\mathbf{H}_k\mathbf{P}_k^-\mathbf{H}_k^T + \mathbf{R}_k\right)^{-1} \\
\hat{\mathbf{X}}_k^- &= \left(\mathbf{I} + \mathbf{F}_{k-1}\right)\hat{\mathbf{X}}_{k-1}^+ - \mathbf{F}_{k-2}\hat{\mathbf{X}}_{k-2}^+ + \mathbf{G}_{k-1}\mathbf{u}_{k-1} - \mathbf{G}_{k-2}\mathbf{u}_{k-2} \\
\hat{\mathbf{X}}_k^+ &= \hat{\mathbf{X}}_k^- + \mathbf{K}_k\left(\mathbf{Y}_k - \mathbf{H}_k\hat{\mathbf{X}}_k^-\right) \\
\mathbf{P}_k^+ &= \left(\mathbf{I} - \mathbf{K}_k\mathbf{H}_k\right)\mathbf{P}_k^-,
\end{aligned} \tag{37}$$

where $\mathbf{S}_{k-1}$ is calculated by Eq. (38):

$$\begin{aligned}
\mathbf{S}_{k-1} &= E\left[\left(\mathbf{X}_{k-1} - \hat{\mathbf{X}}_{k-1}^+\right)\left(\mathbf{X}_{k-2} - \hat{\mathbf{X}}_{k-2}^+\right)^T\right] = \left(\mathbf{I} - \mathbf{K}_{k-1}\mathbf{H}_{k-1}\right) \\
&\quad \times \left[\left(\mathbf{I} + \mathbf{F}_{k-2}\right)\mathbf{P}_{k-2}^+ - \mathbf{F}_{k-3}\mathbf{S}_{k-2}^T - \mathbf{Q}_{k-3}\left(\mathbf{I} - \mathbf{K}_{k-2}\mathbf{H}_{k-2}\right)^T\right] \\
\mathbf{S}_1 &= \mathbf{P}_1.
\end{aligned} \tag{38}$$

Utilizing the SKF method described above, WiFi and MEMS positioning results can be integrated. In this paper, the corresponding Kalman filter system is originally designed as follows.

The state vector is written as

$$\mathbf{X}_k = \left[x_k\, y_k\right]^T, \tag{39}$$

where x, y are position coordinates of the MU.

The system model is as follows:

$$\begin{cases} x_k = x_{k-1} + c\left(x_{\mathrm{WiFi},k} - x_{\mathrm{WiFi},k-1}\right) + (1-c)\left(x_{\mathrm{MEMS},k} - x_{\mathrm{MEMS},k-1}\right) + b_{x,k-1} + w_{x,k-1} \\ y_k = y_{k-1} + c\left(y_{\mathrm{WiFi},k} - y_{\mathrm{WiFi},k-1}\right) + (1-c)\left(y_{\mathrm{MEMS},k} - y_{\mathrm{MEMS},k-1}\right) + b_{y,k-1} + w_{y,k-1} \end{cases}, \tag{40}$$

where $x_{\mathrm{WiFi}}, y_{\mathrm{WiFi}}$ are position coordinates from WiFi results, $x_{\mathrm{MEMS}}, y_{\mathrm{MEMS}}$ are position coordinates from MEMS results, b_x, b_y are unknown inputs, w_x, w_y are noise, and c is a constant parameter ($0 \le c \le 1$).

Table 1 WiFi test results

Method	Running time (s)	Average positioning error (m)
Traditional WKNN	1.18	1.3248
WKNN + searching space limiting + mean filter	0.79	0.9528

Table 2 MEMS test results

Method	Average positioning error (m)
Traditional EKF	8.2852
EKF + correlated noise	0.9534

The measurement vector is written as

$$\mathbf{Y}_k = \begin{bmatrix} dx_{\mathrm{WiFi},k} + (1-d)x_{\mathrm{MEMS},k} \\ dy_{\mathrm{WiFi},k} + (1-d)y_{\mathrm{MEMS},k} \end{bmatrix}, \tag{41}$$

where d is a constant parameter ($0 \le d \le 1, d \ne c$).

The measurement model is as follows:

$$\mathbf{Y}_k = \mathbf{X}_k + \mathbf{v}_k, \tag{42}$$

where $\mathbf{v}_k$ is the noise.

6 Experiment Description and Results

To evaluate the performance of the proposed indoor navigation approach, several experiments were conducted. The experiments were performed in the second floor of Block C, New Main Building at Beihang University. The size of the test area is around $110 \times 30\ \mathrm{m}^2$. There were 326 RPs and 319 positioning points in all. The position coordinates of the starting point of the MU are (0, 0), and the corresponding heading, pitching, and roll angles are (0, 0, 0).

Table 3 Positioning errors

	Maximum (m)	Mean (m)	RMS (m)
WiFi	2.7507	0.9528	1.1682
MEMS	2.1610	0.9534	1.1574
WiFi/MEMS	1.5436	0.6086	0.7015

In the WiFi part, the detailed positioning accuracy of different algorithms is listed in Table 1. As shown, the running time and average positioning error of traditional WKNN algorithm are 1.18 s and 1.3248 m, respectively. When using the searching space limiting method and mean filter, the running time on the same device and average positioning error are 0.79 s and 0.9528 m, respectively. Therefore, when applying the proposed WiFi-based navigation algorithm, the running time decreases by 33% and the average positioning error decreases by 28%.

In the MEMS part, the detailed positioning accuracy of different algorithms is compared in Table 2. As depicted, the average positioning error of the proposed PDR-based navigation algorithm (using the EKF with correlated noise) reduces to 0.9534 m compared with 8.2852 m of traditional attitude determination EKF algorithm, showing great improvement.

In WiFi/MEMS integration, the SKF-based approach is applied to the originally designed Kalman filter system. The corresponding parameters are set at

$$\mathbf{Q}_k = diag\left(\begin{bmatrix} 1 & 1 \end{bmatrix}\right);$$

$$\mathbf{R}_k = \mathrm{diag}\left(\begin{bmatrix} 1 & 1 \end{bmatrix}\right);$$

$$\hat{\mathbf{X}}_0^+ = \begin{bmatrix} 0 & 0 \end{bmatrix}^T;$$

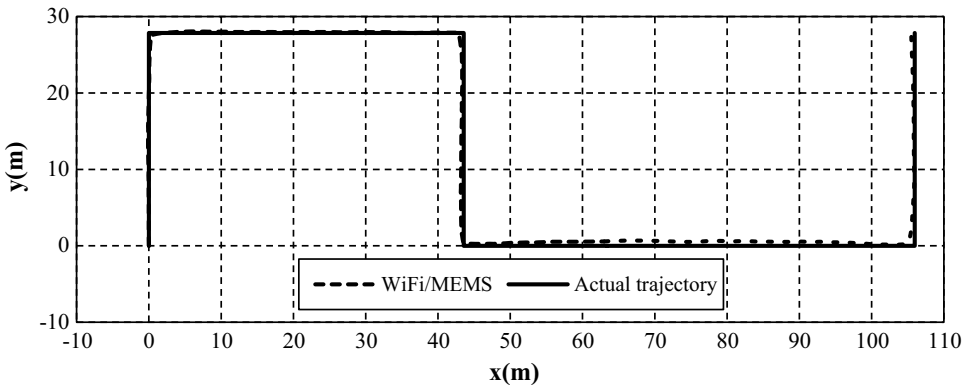

Fig. 4 WiFi/MEMS positioning results

$\mathbf{P}_0^+ = \mathrm{diag}\left(\left[\,0.01\;\;0.01\,\right]\right);$

$c = 0.4; \quad d = 0.55.$

WiFi/MEMS positioning results (with "searching space limiting," "mean filter," "correlated noise," and "SKF-based integration") are depicted in Fig. 4. As shown, the WiFi/MEMS trajectory fits the actual one well.

The detailed estimation errors of WiFi/MEMS illustrated above, WiFi (with "searching space limiting" and "mean filter"), and MEMS (with "correlated noise") are listed in Table 3. As shown, the maximum error, the mean error, and the root mean square (RMS) of position errors are the smallest when using WiFi/MEMS. Therefore, WiFi/MEMS results give the best performance among the three algorithms. The maximum error of WiFi/MEMS is 1.5436 m, which is 56.12% of WiFi and 71.43% of MEMS. The mean error of WiFi/MEMS is 0.6086 m, which is 63.87% of WiFi and 63.83% of MEMS. The RMS of WiFi/MEMS position errors is 0.7015 m, which is 60.05% of WiFi and 60.61% of MEMS.

Furthermore, the error probabilities of these algorithms are depicted in Fig. 5. As shown, the performance of WiFi/MEMS is the best of the three. The cumulative error percentages of WiFi and MEMS are close. In all, this figure proves the advantage of the SKF-based WiFi/MEMS integration approach as well.

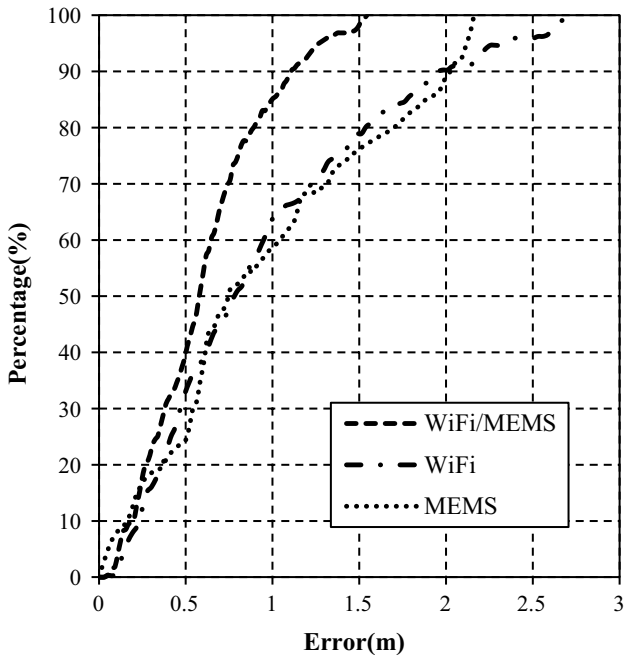

Fig. 5 Cumulative error percentages

Table 4 Positioning errors using different numbers of APs

	Maximum (m)	Mean (m)	RMS (m)
20 APs	1.5436	0.6086	0.7015
17 APs	2.1791	0.6067	0.7149
14 APs	1.8508	0.5946	0.6945
11 APs	1.7181	0.6142	0.7202
8 APs	1.8795	0.6702	0.7830

To further optimize the navigation performance of the proposed WiFi/MEMS solution, the number of selected APs is varied and WiFi/MEMS positioning results in different conditions are compared. The detailed estimation errors using different numbers of APs are listed in Table 4. As shown, the maximum error is the smallest when using 20 APs, while the mean error and the RMS of position errors are the smallest when using 14 APs (0.5946 m and 0.6945 m, respectively), which means positioning results using 14 APs have the optimal navigation performance. Since the computation time gets shorter when fewer APs are selected, using 14 APs instead of 20 APs is suggested in the current study.

7 Conclusion

This paper proposes a novel improved integrated WiFi/MEMS indoor navigation solution. In WiFi part, a novel searching space limiting approach is originally presented. With searching space limiting and a mean filter, the average positioning error decreases by 28% and the running time decreases by 33% compared with the traditional WKNN method. For PDR solution, an attitude determination EKF with correlated process and measurement noise is presented utilizing the information from triaxial gyroscopes and accelerometers. Through this filter, accurate heading calculation is obtained and the average positioning error decreases greatly. In WiFi/MEMS integration, the SKF approach is introduced into indoor navigation field and a novel Kalman filter system is originally designed to achieve higher accuracy.

With these improvements, the WiFi/MEMS trajectory fits the actual one well in the conducted experiments. The average positioning error of the proposed WiFi/MEMS algorithm is less than 0.6 m when 14 APs are selected. As a result, the proposed WiFi/MEMS integration has been proven in indoor tests, and its performance is illustrated to be very competitive for indoor navigation. Furthermore, it has an easy application on smartphones and a broad market prospect.

Acknowledgements This work was sponsored by the National Natural Science Foundation of China (Grant No. 11,501,022). The authors fully appreciate the financial support. The authors would like to thank the reviewers and the editor for many valuable suggestions that helped improve this paper.

References

1. Ezani, M.F.M.; Abdullah, M.A.; Haseeb, S.: A region-to-point indoor localization approach via RSS-magnetic fingerprinting. In: Proceeding of the 5th International Conference on Information and Communication Technology for The Muslim World (ICT4 M), Kuching, Malaysia (2014)
2. Bahl, P.; Padmanabhan, V.N.: RADAR: An in-building RF-based user location and tracking system. In: Proceeding of the IEEE INFOCOM 2000, Tel Aviv, Israel (2000)
3. Youssef, M.; Agrawala, A.: The Horus WLAN location determination system. In: Proceedings of the 3rd International Conference on Mobile Systems, Applications, and Services (MobiSys), Seattle, WA, USA (2005)
4. Rahim, A.: Heading drift mitigation for low-cost inertial pedestrian navigation. Ph.D. dissertation, Dept. Geospat., Univ. Nottingham, Nottingham, UK (2012)
5. Tian, Z.; Fang, X.; Zhou, M.; Li, L.: Smartphone-based indoor integrated WiFi/MEMS positioning algorithm in a multi-floor environment. Micromach **6**(3), 347–363 (2015)
6. Li, F.; Zhao, C.; Ding, G.; Gong, J.; Liu, C.; Zhao, F.: A reliable and accurate indoor localization method using phone inertial sensors. In: Proceedings of the 2012 ACM Conference on Ubiquitous Computing (UbiComp), Pittsburgh, PA, USA (2012)
7. Chung, J.; Donahoe, M.; Schmandt, C.; Kim, I.: Indoor location sensing using geo-magnetism. In: Proceedings of the 9th International Conference on Mobile Systems, Applications, and Services. (MobiSys), Bethesda, MD, USA (2011)
8. Kim, S.J.; Kim, B.K.: Dynamic ultrasonic hybrid localization system for indoor mobile robots. IEEE Trans. Ind. Electron. **60**(10), 4562–4573 (2013)
9. Saab, S.S.; Nakad, Z.S.: A standalone RFID indoor positioning system using passive tags. IEEE Trans. Ind. Electron. **58**(5), 1961–1970 (2011)
10. Yoon, S.; Lee, K.; Rhee, I.: FM-based indoor localization via automatic fingerprint DB construction and matching. In: Proceeding of the 11th Annual International Conference on Mobile Systems, Applications, and Services (MobiSys), Taipei, China (2013)
11. Shu, Y.; Huang, Y.; Zhang, J.; Coué, P.; Cheng, P.; Chen, J.; Shin, K.G.: Gradient-based fingerprinting for indoor localization and tracking. IEEE Trans. Ind. Electron. **63**(4), 2424–2433 (2016)
12. Li, B.; Wang, Y.; Lee, H.K.; Dempster, A.; Rizos, C.: Method for yielding a database of location fingerprints in WLAN. IEE Proc. Commun. **152**(5), 580–586 (2005)
13. Shin, B.; Lee, J.H.; Lee, T.; Kim, H.S.: Enhanced weighted K-nearest neighbor algorithm for indoor Wi-Fi positioning systems. Int. J. Netw. Comput. Adv. Inf. Manage. **2**(2), 15–21 (2012)
14. Wang, B.; Zhao, Y.; Zhang, T.; Hei, X.: An improved integrated fingerprint location algorithm based on WKNN. In: Proceedings of the 29th Chinese Control and Decision Conference, Chongqing, China, pp. 4580–4584 (2017)
15. Jiang, P.; Zhang, Y.; Fu, W.; Liu, H.; Su, X.: Indoor mobile localization based on Wi-Fi fingerprint's important access point. Int. J. Distrib. Sensor Netw. **11**, 429104 (2015)
16. Li, Y.; Zhuang, Y.; Zhang, P.; Lan, H.; Niu, X.; El-Sheimy, N.: An improved inertial/wifi/magnetic fusion structure for indoor navigation. Inf. Fusion **34**, 101–119 (2016)
17. Shaeffer, D.K.: MEMS inertial sensors: a tutorial overview. IEEE Commun. Mag. **51**(4), 100–109 (2013)
18. Wu, Y.; Hu, X.; Hu, D.; Li, T.; Lian, J.: Strapdown inertial navigation system algorithms based on dual quaternions. IEEE Trans. Aerosp. Electron. Syst. **41**(1), 110–132 (2005)
19. Gao, Z.; Mu, D.; Zhong, Y.; Gu, C.: A strap-down inertial navigation/spectrum red-shift/star sensor (SINS/SRS/SS) autonomous integrated system for spacecraft navigation. Sensors **18**(7), 1–16 (2018)
20. Zhao, P.; Pan, S.; Ye, F.; Lin, X.; Zhang, J.; Cao, X.: Research on the detection technology based on INSGNSS for the dynamic positioning performance of satellite navigation terminals. In: Proceedings of the China Satellite Navigation Conference, (CSNC), Harbin, China (2018)
21. Yu, J.; Na, Z.; Liu, X.; Deng, Z.: WiFi/PDR-integrated indoor localization using unconstrained smartphones. EURASIP J. Wirel. Commun. **2019**, 1–13 (2019)
22. Cho, H.H.; Kim, M.; Kim, S.: A study on PDR heading angle error correction algorithm using WLAN based localization information. In: Proceedings of the 7th International Conference Embedded and Multimedia Computing Technology and Service (EMC), Gwangju, Korea (2012)
23. Raitoharju, M.; Nurminen, H.; Piché, R.: Kalman filter with a linear state model for PDR + WLAN positioning and its application to assisting a particle filter. EURASIP J. Adv. Signal Process. **2015**, 1–13 (2015)
24. Lan, H.; Yu, C.; El-Sheimy, N.: An integrated PDR/GNSS pedestrian navigation system. In: Proceedings of the China Satellite Navigation Conference (CSNC), Xian, China (2015)
25. Zhuang, Y.; El-Sheimy, N.: Tightly-coupled integration of WiFi and MEMS sensors on handheld devices for indoor pedestrian navigation. IEEE Sens. J. **16**(1), 224–234 (2016)
26. Zhuang, Y.; Li, Y.; Qi, L.; Lan, H.; Yang, J.; El-Sheimy, N.: A two-filter integration of MEMS sensors and WiFi fingerprinting for indoor positioning. IEEE Sens. J. **16**(13), 5125–5126 (2016)
27. Cui, Y.; Zhang, Y.; Huang, Y.; Wang, Z.; Fu, H.: Novel WiFi/MEMS integrated indoor navigation system based on two-stage EKF. Micromach. **10**(3), 1–21 (2019)
28. Khodayari, S.; Maleki, M.; Hamedi, E.: A RSS-based fingerprinting method for positioning based on historical data. In: Proceedings of the 2010 International Symposium on Performance Evaluation of Computer and Telecommunication Systems, Ottawa, ON, Canada, pp. 306–310 (2010)
29. Lau, E.E.L.; Chung, W.Y.: Enhanced RSSI-based real-time user location tracking system for indoor and outdoor environments. In: Proceedings of the International Conference on Convergence Information Technology, pp. 1213–1218 (2007)
30. Fang, S.H.; Lin, T.N.; Lee, K.C.: A novel algorithm for multipath fingerprinting in indoor WLAN environments. IEEE Trans. Wireless Commun. **7**(9), 3579–3588 (2008)
31. Li, J.; Fu, J.; Li, A.; Bao, W.; Gao, Z.: An improved WKNN indoor fingerprinting positioning algorithm based on adaptive hierarchical clustering. In: Proceedings of the International Conference on Life System Modeling and Simulation (LSMS) and International Conference on Intelligent Computing for Sustainable Energy and Environment, (ICSEE), Nanjing, China (2017)
32. Li, C.; Qiu, Z.; Liu, C.: An improved weighted K-nearest neighbor algorithm for indoor positioning. Wireless Pers. Commun. **96**(2), 2239–2251 (2017)
33. Battiti, R.; Nhat, T.L.; Villani, A.: Location-aware computing: A neural network model for determining location in wireless LANs. Dep. Inf. Commun. Technol., Univ. Trento, Trento, Italy, Tech. Rep. # DIT-02-0083 (2002)
34. Fang, S.H.; Lin, T.N.: Indoor location system based on discriminant-adaptive neural network in IEEE 80211 environments. IEEE Trans. Neural Netw. **19**(11), 1973–1978 (2008)

35. Wu, X.; Kumar, V.; Quinlan, J.R.; Ghosh, J.; Yang, Q.; Motoda, H.; McLachlan, G.J.; Ng, A.; Liu, B.; Yu, P.S.; Zhou, Z.; Steinbach, M.; Hand, D.J.; Steinberg, D.: Top 10 algorithms in data mining. Knowl. Inf. Syst. **14**(1), 1–37 (2008)
36. Li, C.; Gu, Y.; Yu, G.; Li, F.: wNeighbors: A method for finding k nearest neighbors in weighted regions. In: Proceedings of the International Conference on Database Systems for Advanced Applications (DASFAA), Hong Kong, China (2011)
37. Guvenc, I.; Abdallah, C.T.; Jordan, R.; Dedeoglu, O.: Enhancements to RSS based indoor tracking systems using Kalman filters. In: Proceedings of the International Signal Process on Conference Global, Expo, Dallas, TX, USA (2003)
38. Zhou, J.; Yeung, W.M.; Ng, J.K.: Enhancing indoor positioning accuracy by utilizing signals from both the mobile phone network and the wireless local area network. In: Proceedings of the 22nd, International Conference on Advanced Information Networking and Applications, Gino-wan City, Japan, pp. 138-145 (2008)
39. Ni, L.M.; Liu, Y.; Lau, Y.C.; Patil, A.P.: LANDMARC: Indoor location sensing using active RFID. In: Proceedings of the 1st IEEE International Conference on Pervasive Computing Communication, Fort Worth, TX, USA (2003)
40. Fu, H.: Inverse regression analysis and data fusion. J. Mech. Strength **24**(4), 518–523 (2002)
41. Simon, D.: Optimal State Estimation: Kalman, H Infinity, and Nonlinear Approaches. Wiley, Hoboken (2006)
42. Fu, H.; Wu, Y.; Lou, T.; Xiao, Q.: Self-calibration Kalman filter method. J. Aerosp. Power **29**(6), 1363–1368 (2014)